

1 **Comparative analysis of network-based measures for the**
2 **assessment of drug-induced liver injury: A case study of**
3 ***Hypericum perforatum***

4 Antony Bevan^{1,*}

¹Department of Pharmacognosy, Madurai Medical College, Madurai, India

*Corresponding author: antonybevan04@gmail.com

5 **Abstract**

6 Network proximity is widely used to prioritize compound–disease associations, yet proximity Z-scores
7 are sensitive to target set size, network density, and network construction parameters. While often in-
8 terpreted as functional indicators, these metrics are susceptible to inferential instability, where ranking
9 significance is driven by target-count-dependent null distributions rather than physical reachability.

10 Here, we systematically evaluate the robustness of proximity-based and influence-based metrics
11 using a liver-expressed human protein–protein interaction network. Using two constituents of *Hyper-*
12 *icum perforatum* as a controlled comparison, we show that proximity-based rankings are unstable and
13 threshold-dependent. Although Quercetin (62 targets) achieves higher proximity Z-scores than Hyper-
14 forin (10 targets) in high-confidence networks, this significance is an artifact of the law of large numbers
15 acting on the null distribution. In physical distance space, Hyperforin is closer to drug-induced liver
16 injury (DILI) genes, a ranking that is stably captured by random walk–based influence propagation.

17 We quantify this disparity by calculating the average influence per target, revealing that Hyperforin
18 achieves 3.7-fold greater efficiency in DILI-module perturbation than Quercetin. This efficiency ad-
19 vantage remains robust across topology-only and expression-weighted analyses, as well as bootstrap
20 resampling and chemical similarity controls. Our results demonstrate that proximity Z-scores may lead
21 to misleading prioritizations when target set sizes differ, and that influence-based propagation provides a
22 more robust and theoretically consistent framework for network toxicology. More broadly, this work pro-
23 vides a methodological template for identifying and correcting metric artifacts in polypharmacological

24 risk assessment.

25 **Keywords:** network propagation, proximity metrics, metric robustness, drug-induced liver injury, polyphar-
26 macology, Z-score confounding, perturbation efficiency.

27

1 Introduction

28 Network-based drug safety assessment commonly utilizes proximity to disease-associated genes as a
29 prioritization criterion, assuming that compounds with more targets or closer network positions pose
30 greater risk [Hopkins, 2008, Barabási et al., 2011, Guney et al., 2016, Menche et al., 2015]. This intu-
31 ition is attractive due to its computational simplicity and interpretability. However, proximity rankings
32 are typically reported as Z-scores relative to degree-matched null models. While Z-scores are intended
33 to quantify statistical significance, they are fundamentally sensitive to target set size: as the number of
34 targets increases, the variance of the null distribution decreases (the Law of Large Numbers), leading
35 to inflated significance for compounds with broad polypharmacology. Whether such "inferential sig-
36 nificance" reflects true biological influence, or whether it introduces systematic bias into toxicological
37 prioritization, remains a critical question.

38 *Hypericum perforatum* (St. John's Wort) offers a sharp stress test for this question. The extract con-
39 tains two bioactive constituents with contrasting pharmacological profiles: Hyperforin (10 validated tar-
40 gets, potent PXR activator) and Quercetin (62 targets, broad polypharmacology) [Nahrstedt and Butter-
41 weck, 1997, Moore et al., 2000, Boots et al., 2008]. Conventional network analysis, relying on proximity
42 Z-scores, would predict greater DILI-associated risk for Quercetin despite Hyperforin's well-established
43 role in clinical hepatotoxicity through PXR-mediated enzyme induction. This system therefore allows
44 us to evaluate whether proximity-based prioritization is stable across network construction parameters or
45 whether it is confounded by target-count artifacts.

46 In this study, we systematically evaluate the robustness of proximity-based and influence-based met-
47 rics. We demonstrate that proximity Z-scores yield unstable, threshold-dependent rankings that are
48 driven by null-distribution tightening rather than physical distance. To resolve this, we utilize random
49 walk-based influence propagation, which integrates over all paths weighted by transition probability
50 and captures signal amplification through regulatory hubs [Köhler et al., 2008]. We utilize probability-
51 normalized influence mass to quantify perturbation efficiency, and use bootstrap resampling to exclude
52 target-count confounding. Our results demonstrate that influence-based propagation provides a more
53 stable and mechanistically aligned framework for comparative network toxicology, particularly when

54 comparing compounds with asymmetric target sets.

55 2 Results

56 2.1 Proximity Z-scores are confounded by target set size

57 We first established network context by quantifying target count and shortest-path proximity to 82 DILI-
58 associated genes (Figure 1). Quercetin engages 62 targets in the liver-expressed largest connected
59 component; Hyperforin engages 10. At STRING confidence ≥ 900 , Hyperforin targets are physically
60 closer to DILI genes ($d_c = 1.30$) than Quercetin targets ($d_c = 1.68$; Table 1). However, the proxim-
61 ity Z-scores yield the opposite ranking: Quercetin achieves $Z = -5.44$ ($p < 0.001$), while Hyperforin
62 achieves $Z = -3.86$ ($p < 0.001$). All reported associations survived Benjamini–Hochberg FDR correc-
63 tion ($q < 0.05$).

64 This discrepancy highlights a fundamental confounder in proximity Z-scores: the law of large num-
65 bers. As target set size increases, the variance of the null distribution decreases ($\sigma_{null} = 0.09$ for
66 Quercetin vs 0.24 for Hyperforin), inflating the significance of broader target sets despite greater phys-
67 ical distance. This statistical artifact suggests that Quercetin poses greater risk, whereas the physical
68 topology favors Hyperforin.

69 2.2 Influence-based rankings are stable and resolve the confound

70 Random walk with restart (RWR) stabilizes this ranking by integrating over all paths (Figure 2). Hyper-
71 forin achieves influence $Z = +10.12$ ($p < 0.001$); Quercetin achieves $Z = +4.55$ ($p < 0.001$; Table 1).
72 Unlike proximity, influence Z-scores correctly reflect the topological advantage of Hyperforin’s regula-
73 tory hub occupancy. The ranking remains consistent across topology-only and expression-weighted anal-
74 yses, demonstrating that influence propagation is less susceptible to sample-size artifacts than shortest-
75 path distance.

76 2.3 Expression weighting refines the signal

77 To assess whether the RWR signal persists under tissue-specific constraint, we applied expression-
78 weighted influence propagation (EWI), weighting transitions by destination-node liver expression (Fig-
79 ure 3).

80 The Z-score differential narrows but remains substantial under expression weighting: Hyperforin
81 $Z = +8.98$ ($p < 0.001$); Quercetin $Z = +5.79$ ($p < 0.001$). Hyperforin’s advantage is driven primarily

82 by the PXR–CYP master regulatory axis, which remains highly active in liver tissue (e.g., CYP3A4 at
83 335 TPM). Quercetin’s influence is moderated by its broad, diffuse target profile, which includes several
84 high-expression nodes (e.g., CFB at 1,115 TPM) that do not converge on a DILI effector hub.

85 **2.4 Normalizing for target count confirms Hyperforin’s topological advantage**

86 To resolve the target-count paradox, we compared the average network influence of each individual
87 target, reframing polypharmacology as an efficiency problem rather than a coverage problem (Figure 4;
88 Table 2).

Compound	Targets	Eff. (RWR)	Eff. (EWI)	RWR Ratio*	EWI Ratio†
Hyperforin	10	0.1138	0.1330	—	—
Quercetin	62	0.0322	0.0493	—	—
Fold difference	—	—	—	3.5× (3.7×)	2.7× (2.8×)

90 *RWR Ratio: observed ratio (robust ratio in parentheses). †EWI Ratio: observed ratio (robust ratio in paren-
91 theses).

92 Each Hyperforin target contributes 3.7× more DILI-directed influence than each Quercetin target (robust ra-
93 tio). This disparity indicates that Hyperforin’s target positions are substantially higher leverage than those of
94 Quercetin, achieving greater perturbation efficiency despite a 6-fold smaller target set.

95 **2.5 Bootstrap resampling excludes target-selection bias**

96 To rule out the possibility that Hyperforin’s advantage arises from favorable target selection rather than strategic
97 network positioning, we performed bootstrap sensitivity analysis (Figure 5). 100 random 10-target subsets were
98 sampled without replacement from Quercetin’s 62-target pool and scored by RWR.

99 Hyperforin’s observed influence (0.1138) exceeds the entire bootstrap distribution from Quercetin (mean =
100 0.0308, 95% CI = [0.0160, 0.0542]; Table 3). The fold difference between Hyperforin and the bootstrap mean is
101 3.7×. This confirms that Hyperforin’s advantage is not an artifact of target count; even when sampling equalized
102 subsets from Quercetin’s pool, no configuration matches Hyperforin’s influence.

103 **2.6 Ranking stability across network thresholds**

104 The influence ranking is stable across network confidence thresholds (Table 6). Hyperforin ranks first in all RWR
105 and EWI configurations at both ≥ 700 and ≥ 900 thresholds. Notably, the proximity ranking reverses between
106 thresholds: at ≥ 700 , Hyperforin is physically closer ($d_c = 0.60$ vs 1.34) and more "significant" ($Z = -6.04$ vs

107 -5.46). At ≥ 900 , Quercetin appears more "significant" ($Z = -5.44$ vs -3.86) despite being physically more dis-
108 tant (1.68 vs 1.30). This instability in proximity Z-scores—while influence rankings remain stable—demonstrates
109 that influence-based metrics are more robust to network construction parameters.

110 **2.7 Chemical similarity excludes structural confounding**

111 To exclude the possibility that Hyperforin's network signal reflects structural similarity to known hepatotoxins,
112 we performed chemical similarity analysis against the DILIrank reference set (Figure 6). Morgan fingerprints
113 (ECFP4) revealed that neither compound exceeds the 0.4 Tanimoto threshold for structural analog detection. No-
114 tably, Quercetin exhibits higher structural similarity to DILI reference drugs yet lower network influence, reinforc-
115 ing that the observed asymmetry is driven by network topology rather than chemical features.

116 **3 Discussion**

117 **3.1 Robustness and the Z-score confound**

118 The central finding of this study is the inherent instability of network proximity Z-scores when comparing com-
119 pounds with asymmetric target set sizes. While proximity is often used for prioritization, we demonstrate that
120 its significance rankings are fundamentally confounded by the law of large numbers. As the number of targets
121 increases, the variance of the null distribution (σ_{null}) decreases, making even modest topological distances appear
122 highly significant. This is clearly observed in our comparison: at STRING ≥ 900 , Quercetin (62 targets) achieves
123 a more significant proximity Z-score than Hyperforin (10 targets) despite being physically more distant ($d_c = 1.68$
124 vs 1.30). This statistical artifact disappears when considering influence-based metrics, which correctly identify
125 Hyperforin as the high-leverage modulator.

126 Critically, the proximity Z-score ranking is threshold-dependent. At ≥ 700 , Hyperforin is physically closer and
127 more significant; at ≥ 900 , the physical advantage persists, but the significance ranking reverses due to the tighter
128 Quercetin null. This instability indicates that proximity Z-scores are unreliable for comparative prioritization.
129 In contrast, influence-based rankings (RWR and EWI) remain stable across multiple STRING confidence tiers,
130 correctly prioritizing the regulatory hub modulator (Hyperforin) in all configurations.

131 The mechanistic explanation for this robustness is that RWR integrates over *all* paths, capturing how signals
132 amplify through hubs like PXR and AKT1. Shortest-path proximity, by contrast, is a descriptive metric for min-
133 imum reachability; treating it as an inferential surrogate for functional impact conflates topological context with
134 biological consequence.

135 **3.2 Expression weighting as a biological constraint**

136 Expression-weighted influence (EWI) constrains signal propagation to liver-active nodes. By attracting signal to
137 highly expressed proteins (destination-node weighting), we ensure that the network propagation reflects tissue-

138 specific biology. Under this constraint, the Hyperforin advantage persists, demonstrating that its topological ef-
139 ficiency is not an artifact of an unconstrained PPI network but is supported by the expression profile of the liver.
140 Attenuation of signal is expected when walks are constrained to active pathways; the fact that the ranking remains
141 stable provides positive evidence for the biological relevance of the PXR axis.

142 **3.3 Perturbation efficiency vs. topological coverage**

143 By normalizing total influence for target set size (where the restart vector is already $|T|$ -weighted), we provide
144 a more balanced comparison of perturbation efficiency. Our results show that a single Hyperforin target exerts
145 3.7-fold more influence on the DILI module than a Quercetin target.

146 This efficiency claim is further validated by bootstrap sensitivity analysis. Even when sampling size-matched
147 10-target subsets from Quercetin’s pool, none reached the influence level achieved by Hyperforin. This demon-
148 strates that the advantage is not due to target count, but to the strategic network position of Hyperforin’s tar-
149 gets—specifically their convergence on the PXR master regulator and downstream CYP effectors.

150 **3.4 Mechanistic context: The PXR axis**

151 The stability of the influence ranking aligns with the well-characterized PXR–CYP master regulatory axis. Hyper-
152 forin’s primary target, NR1I2 (PXR), induces the expression of major xenobiotic metabolism enzymes including
153 CYP3A4 and CYP2C9 [Moore et al., 2000, Watkins et al., 2001]. In our network analysis, these effectors are
154 part of the target set and the DILI module, creating a high-connectivity hub structure that enables efficient prop-
155 agation. Quercetin’s 62 targets, while numerous, are distributed across redundant or peripheral pathways that do
156 not converge on a regulatory bottleneck. Furthermore, clinical evidence indicates that Quercetin is not associated
157 with hepatotoxicity and may exhibit hepatoprotective properties [Boots et al., 2008, National Institute of Diabetes
158 and Digestive and Kidney Diseases, 2020]. Recent experimental studies have corroborated that St. John’s wort
159 exacerbates hepatotoxicity through precisely this PXR-mediated bioactivation mechanism [Chen et al., 2022].

160 **3.5 Limitations and Conclusions**

161 While our findings favor influence-based metrics, we acknowledge that network influence is a measure of topolog-
162 ical reach and perturbation potential, not a direct surrogate for actual toxicological outcomes. This model is dose-
163 independent and does not account for pharmacokinetics, binding affinity, or saturation kinetics. A high influence
164 score indicates that a compound’s targets are strategically positioned to modulate a disease module—representing a
165 measure of systemic susceptibility—but the actual biological effect depends on the molecular mechanism of action
166 (e.g., agonism vs. antagonism) and the kinetic context. In this study, we utilized *H. perforatum* as a known toxicolo-
167 gical model to validate the *reliability* of the metrics themselves; the biological ground truth (Hyperforin-mediated
168 PXR activation) allowed us to confirm that influence propagation correctly identifies high-leverage perturbations
169 where proximity metrics fail. Future work integrating kinetic modeling or structural binding energy will be re-

170 required to translate topological susceptibility into definitive risk predictions.

171 The methodological conclusion remains: proximity Z-scores are susceptible to sample-size confounding and
172 should be used descriptively rather than for comparative inference. Influence-based propagation provides a more
173 stable framework that survives robustness checks and aligns better with mechanistic reality.

174 In conclusion, we provide a methodological template for identifying and resolving metric artifacts in network
175 toxicology. By shifting the focus from topological coverage to perturbation efficiency, and from significance-driven
176 Z-scores to robustness-checked influence, we enable more precise risk attribution in complex polypharmacological
177 systems. Furthermore, this work provides a foundation for developing network models with improved mechanistic
178 interpretability. By integrating signed edge weights and transcriptometric data, future iterations of this framework
179 could investigate phenotype-specific associations, potentially linking topological influence on specific biological
180 sub-modules to discrete clinical outcomes such as cholestasis or steatosis.

181 4 Methods

182 4.1 Data sources

183 4.1.1 Protein–protein interaction network

184 Human protein–protein interactions were obtained from STRING v12.0 [Szklarczyk et al., 2023]. Combined
185 confidence scores were computed per STRING methodology (text mining, experiments, databases, co-expression,
186 neighborhood, gene fusion, co-occurrence). Only edges with combined confidence ≥ 900 (highest confidence tier)
187 were retained. Raw network: 11,693 genes, 100,383 edges.

188 4.1.2 Liver expression data

189 Gene expression data were obtained from the Genotype-Tissue Expression Project (GTEx) v8 [GTEx Consortium,
190 2020]. Median transcripts per million (TPM) values for liver tissue were extracted from the 2017-06-05 release
191 (RNASeQCv1.1.9). Genes with liver TPM ≥ 1 were retained. Result: 13,496 liver-expressed genes.

192 4.1.3 Drug-induced liver injury gene set

193 DILI-associated genes were obtained from DisGeNET [Piñero et al., 2020] curated gene-disease associations.
194 Query: UMLS concept identifier C0860207 (Drug-Induced Liver Injury). Inclusion criterion: genes with curated
195 evidence linking to DILI. Raw DILI gene count: 127 genes.

196 4.1.4 Hyperforin targets

197 Hyperforin targets were curated from primary literature sources [Moore et al., 2000, Watkins et al., 2001]. Sources
198 included studies of PXR activation, CYP induction, and ABC transporter modulation. Raw target count: 14
199 proteins (Table 7).

200 **4.1.5 Quercetin targets**

201 Quercetin targets were retrieved programmatically from ChEMBL v31 [Mendez et al., 2019] via REST API.
202 Query: CHEMBL159 (Quercetin). Filter: human targets with experimentally validated bioactivity (IC_{50} , K_i ,
203 or $EC_{50} \leq 10 \mu M$). Raw target count: 122 proteins.

204 **4.2 Target processing**

205 Protein identifiers were mapped to HUGO gene symbols using STRING info files and UniProt [UniProt Consor-
206 tium, 2023]. Non-human proteins (mouse, rat, bacterial, viral) were excluded. Gene symbols were standardized
207 (e.g., MDR1 → ABCB1). Processed target counts: Hyperforin = 14, Quercetin = 87.

208 **4.3 Network construction**

209 The STRING network was filtered to genes with liver expression ≥ 1 TPM (GTEx v8). The largest connected
210 component (LCC) was extracted using NetworkX [Hagberg et al., 2008]. Compound targets and DILI genes not
211 present in the LCC were excluded. Final network: 7,677 nodes, 66,908 edges. Final target counts: Hyperforin =
212 10, Quercetin = 62. Final DILI gene count: 82.

213 Five genes are targeted by both compounds: ABCG2, AKT1, CYP3A4, MMP2, MMP9. These were retained
214 in both target sets.

215 **4.4 Shortest-path proximity (descriptive)**

216 Mean minimum shortest-path distance from compound targets T to DILI genes D :

$$d_c = \frac{1}{|T|} \sum_{t \in T} \min_{d \in D} \text{dist}(t, d) \quad (1)$$

217 where $\text{dist}(t, d)$ is the unweighted shortest-path length in the LCC. Shortest-path proximity is a descriptive metric.
218 It was used to provide network context, not to test influence.

219 **4.5 Random walk with restart**

220 Influence propagation was quantified using random walk with restart (RWR) [Köhler et al., 2008, Guney et al.,
221 2016]. Given adjacency matrix \mathbf{A} , the column-normalized transition matrix \mathbf{W} :

$$W_{ij} = \frac{A_{ij}}{\sum_k A_{kj}} \quad (2)$$

222 Steady-state probability vector \mathbf{p} satisfies:

$$\mathbf{p} = (1 - \alpha)\mathbf{W}\mathbf{p} + \alpha\mathbf{p}_0 \quad (3)$$

223 Restart probability: $\alpha = 0.15$. Restart vector: $p_0(i) = 1/|T|$ for $i \in T$, else 0. Convergence criterion: $\|\mathbf{p}^{(k+1)} -$
224 $\mathbf{p}^{(k)}\|_1 < 10^{-6}$. Maximum iterations: 100.

225 Total DILI influence:

$$I = \sum_{d \in D} p(d) \quad (4)$$

226 4.6 Permutation testing

227 Null distributions were generated by sampling 1,000 random target sets. Degree matching: each random target
228 was sampled from nodes with degree within $\pm 25\%$ of the original target's degree. To prevent hash randomization
229 artifacts, target lists were sorted alphabetically before assignment. Z-score:

$$Z = \frac{x_{\text{obs}} - \mu_{\text{null}}}{\sigma_{\text{null}}} \quad (5)$$

230 P -values were computed as the fraction of permuted values \geq the observed value (one-tailed). P -values at the
231 permutation floor ($< 1/1000$) are reported as $p < 0.001$. Multiple testing correction: Benjamini–Hochberg FDR.
232 Random seed: 42.

233 4.7 Expression-weighted influence

234 Edge weights were modified by destination-node liver expression:

$$W'_{ij} = \frac{A_{ij} \cdot e_i}{\sum_k A_{kj} \cdot e_k} \quad (6)$$

235 where e_i is the normalized liver expression for gene i (GTEx v8 liver). Liver TPM values were log-transformed
236 ($\log_2(\text{TPM} + 1)$) and min-max normalized to $[0, 1]$ across the network. A minimum expression floor of 0.01 was
237 applied to ensure all nodes remained reachable. Attracting signal to highly-expressed nodes constrains RWR
238 propagation to biologically active pathways in the liver. All other RWR parameters were identical. Random seed:
239 42.

240 4.8 Quantifying perturbation efficiency

241 By defining the restart vector as $\mathbf{p}_0(i) = 1/|T|$ (Eq. 75), the total steady-state probability mass \mathbf{p} is inherently
242 partitioned among the target set. Consequently, the summed influence I on the DILI module (Eq. 81) represents
243 the average perturbation efficiency per target. This normalization serves as an effect-size adjustment that allows
244 for a direct comparison of the per-unit impact of compounds with asymmetric target sets. Hereafter, we refer to
245 this as the perturbation efficiency.

246 **4.9 Bootstrap sensitivity analysis**

247 To assess whether target count explains the observed ranking: 100 random 10-target subsets were sampled without
248 replacement from Quercetin's 62-target pool. Each subset was scored by standard RWR. Summary statistics: mean,
249 standard deviation, 95th percentile. The observed Hyperforin influence was compared to the bootstrap distribution.
250 Random seed: 42.

251 **4.10 Chemical similarity analysis**

252 Structural similarity to known hepatotoxins was assessed to exclude confounding by chemical class. Morgan
253 fingerprints (ECFP4; radius = 2, 2048 bits) were generated using RDKit v2023.03 [RDKit, 2023]. Reference set:
254 DILIrank 2.0 drugs with retrievable SMILES (542 DILI-positive, 365 DILI-negative). SMILES were retrieved via
255 PubChem REST API. Tanimoto coefficient:

$$\text{Tanimoto}(A, B) = \frac{|A \cap B|}{|A \cup B|} \quad (7)$$

256 Maximum similarity across the reference set was reported for each compound. Structural analog threshold: Tani-
257 moto > 0.4 [Maggiora et al., 2014].

258 **4.11 Software and reproducibility**

259 Python 3.10, NetworkX 3.1 [Hagberg et al., 2008]; R 4.3, igraph 1.5. All random seeds fixed at 42. Target lists
260 sorted alphabetically before processing.

261 **4.12 Code and data availability**

262 All code: <https://github.com/antonybevan/h-perforatum-network-tox>

263 Data sources:

- 264 • STRING v12.0: <https://string-db.org>
- 265 • GTEx v8: <https://gtexportal.org>
- 266 • ChEMBL v31: <https://www.ebi.ac.uk/chembl>
- 267 • DILIrank 2.0: <https://www.fda.gov/science-research/ltrkb>

268 **References**

269 H Assefa and V Butterweck. The role of hyperforin in the metabolic and transport-mediated drug interactions of
270 St. John's wort. *Planta Medica*, 70(4):291–300, 2004. doi: 10.1055/s-2004-818938.

- 271 Albert-László Barabási, Natali Gulbahce, and Joseph Loscalzo. Network medicine: a network-based approach to
272 human disease. *Nature Reviews Genetics*, 12(1):56–68, 2011. doi: 10.1038/nrg2918.
- 273 Agnes W Boots, Guido RMM Haenen, and Aalt Bast. Health effects of quercetin: from antioxidant to nutraceutical.
274 *European Journal of Pharmacology*, 585(2-3):325–337, 2008. doi: 10.1016/j.ejphar.2008.03.008.
- 275 Siyu Chen, Xue Wang, Xinran Ye, Qinjin Wang, Xin Sun, Chunyan Ma, Zhidong Yuan, and Yang Yu. St. John's
276 wort exacerbates acetaminophen-induced liver injury through PXR and CYP-mediated bioactivation. *Toxicological Sciences*, 190(1):68–80, 2022. doi: 10.1093/toxsci/kfac098.
- 278 GTEx Consortium. The GTEx Consortium atlas of genetic regulatory effects across human tissues. *Science*, 369
279 (6509):1318–1330, 2020. doi: 10.1126/science.aaz1776.
- 280 Emre Guney, Jörg Menche, Marc Vidal, and Albert-László Barabasi. Network-based in silico drug efficacy screen-
281 ing. *Nature Communications*, 7:10331, 2016. doi: 10.1038/ncomms10331.
- 282 Aric A Hagberg, Daniel A Schult, and Pieter J Swart. Exploring network structure, dynamics, and function using
283 NetworkX. In Gaël Varoquaux, Travis Vaught, and Jarrod Millman, editors, *Proceedings of the 7th Python in
284 Science Conference (SciPy 2008)*, pages 11–15, 2008.
- 285 M Hennessy, D Kelleher, JP Lloyd, A Alrajhi, O Meenaghan, C McDonald, F Mulcahy, JP Spiers, and J Feely.
286 St John's wort increases expression of P-glycoprotein: implications for drug interactions. *British Journal of
287 Clinical Pharmacology*, 53(1):75–82, 2002. doi: 10.1046/j.1365-2125.2002.01512.x.
- 288 Andrew L Hopkins. Network pharmacology: the next paradigm in drug discovery. *Nature Chemical Biology*, 4
289 (11):682–690, 2008. doi: 10.1038/nchembio.118.
- 290 Katarina Hostanska, J Reiher, S Jessenmeyer, J Reichling, and R Saller. Hyperforin and hypericin: synergistic
291 cytotoxicity and induced apoptosis in human malignant cell lines. *European Journal of Pharmaceutics and
292 Biopharmaceutics*, 55(3):301–310, 2003. doi: 10.1016/s0939-6411(03)00021-3.
- 293 Sebastian Köhler, Sebastian Bauer, Denise Horn, and Peter N Robinson. Walking the interactome for prioritization
294 of candidate disease genes. *The American Journal of Human Genetics*, 82(4):949–958, 2008. doi: 10.1016/j.aj
295 hg.2008.02.013.
- 296 Bernard J Komoroski, Shuyan Zhang, Steven A Wrighton, Stephen C Strom, Raman Venkataraman, and Erin G
297 Schuetz. Induction and inhibition of cytochromes P450 by the St. John's wort constituent hyperforin in human
298 hepatocytes. *Drug Metabolism and Disposition*, 32(5):512–518, 2004. doi: 10.1124/dmd.32.5.512.
- 299 Vikas Kumar, Alexander Mdzinarishvili, Thomas Kiewert, Maria P Abbracchio, Annalisa Pinna, Renata Ciccarelli,
300 Walter E Müller, and Jochen Klein. NMDA receptor-antagonistic properties of hyperforin, a constituent of St.
301 John's wort. *Journal of Pharmacological Sciences*, 102(1):47–54, 2006. doi: 10.1254/jphs.fp06041.

- 302 Kristian Leuner, Viacheslav Kazanski, Marina Müller, Kirill Essin, Britta Henke, Martina Gassen, Christopher
303 Koch, Christina Bulut, Karola Silbermann, Annette Kopp-Schneider, Gerald Thiel, Vladimir Laketa, Inna Gor-
304 shkova, Valentina Przetheskikh, Christian Harteneck, Wolfgang F Graier, Vadym Degtiar, Peter Lipp, Axel
305 Lückhoff, and Walter E Müller. Hyperforin—a key constituent of St. John’s wort specifically activates TRPC6
306 channels. *The FASEB Journal*, 21(14):4101–4111, 2007. doi: 10.1096/fj.07-8110com.
- 307 Gerald Maggiora, Martin Vogt, Dagmar Stumpfe, and Jürgen Bajorath. Molecular similarity in medicinal chem-
308 istry. *Journal of Medicinal Chemistry*, 57(8):3186–3204, 2014. doi: 10.1021/jm401411z.
- 309 Jörg Menche, Amitabh Sharma, Maksim Kitsak, Susan Dina Ghiassian, Marc Vidal, Joseph Loscalzo, and Albert-
310 László Barabasi. Uncovering disease-disease relationships through the incomplete interactome. *Science*, 347
311 (6224):1257601, 2015. doi: 10.1126/science.1257601.
- 312 David Mendez, Anna Gaulton, A Patrícia Bento, Jon Chambers, Marleen De Veij, Eloy Félix, María Paula Magaña,
313 Juan F Mosquera, Prudence Mutowo, Michał Nowotka, Maria Gordillo-Marañón, Fiona Hunter, Laura Junco,
314 Grace Mugumbate, Milagros Rodriguez-Lopez, Francis Atkinson, Nicolas Bosc, Chris J Radoux, Aldo Segura-
315 Cabrera, Anne Hersey, and Andrew R Leach. ChEMBL: towards direct deposition of bioassay data. *Nucleic
316 Acids Research*, 47(D1):D930–D940, 2019. doi: 10.1093/nar/gky1075.
- 317 Linda B Moore, Bryan Goodwin, Stacey A Jones, G Bruce Wisely, Connie J Serabjit-Singh, Timothy M Willson,
318 John L Collins, and Steven A Kliewer. St. John’s wort induces hepatic drug metabolism through activation of
319 the Pregnan X Receptor. *Proceedings of the National Academy of Sciences*, 97(13):7500–7502, 2000. doi:
320 10.1073/pnas.130155097.
- 321 Adolf Nahrstedt and Veronika Butterweck. Biologically active and other chemical constituents of the herb of
322 Hypericum perforatum L. *Pharmacopsychiatry*, 30(S2):129–134, 1997. doi: 10.1055/s-2007-979533.
- 323 National Institute of Diabetes and Digestive and Kidney Diseases. LiverTox: Clinical and research information
324 on drug-induced liver injury [internet]. quercetin. <https://www.ncbi.nlm.nih.gov/books/NBK548281/>,
325 2020. Updated July 10, 2020.
- 326 R Scott Obach. Inhibition of human cytochrome P450 enzymes by constituents of St. John’s Wort, an herbal
327 preparation used in the treatment of depression. *Journal of Pharmacology and Experimental Therapeutics*, 294
328 (1):88–95, 2000. doi: 10.1124/jpet.294.1.88.
- 329 Janet Piñero, Juan Manuel Ramírez-Anguita, Josep Saüch-Pitarch, Francesco Ronzano, Emilio Centeno, Ferran
330 Sanz, and Laura I Furlong. The DisGeNET knowledge platform for disease genomics: 2019 update. *Nucleic
331 Acids Research*, 48(D1):D845–D855, 2020. doi: 10.1093/nar/gkz1021.
- 332 C Quiney, C Billard, C Salanoubat, J D Fourneron, and J P Kolb. Hyperforin inhibits MMP-9 secretion by B-cell
333 chronic lymphocytic leukemia cells. *Leukemia*, 20(8):1514–1521, 2006. doi: 10.1038/sj.leu.2404283.

- 334 C Quiney, C Billard, A M Faussat, C Salanoubat, and J P Kolb. Hyperforin directly inhibits AKT1 kinase activity
335 and promotes apoptosis in AML cells. *Leukemia*, 21(10):2101–2111, 2007. doi: 10.1038/sj.leu.2404834.
- 336 RDKit. RDKit: Open-source cheminformatics. <https://www.rdkit.org>, 2023. Version 2023.03.
- 337 Damian Szkłarczyk, Rebecca Kirsch, Mikaela Koutrouli, Katerina Nastou, Farrokh Mehryary, Radja Hachilif,
338 Annika L Gable, Tao Fang, Nadezhda T Doncheva, Sampo Pyysalo, Peer Bork, Lars J Jensen, and Christian
339 von Mering. The STRING database in 2023: protein–protein association networks and functional enrichment
340 analyses for any sequenced genome of interest. *Nucleic Acids Research*, 51(D1):D483–D489, 2023. doi:
341 10.1093/nar/gkac1000.
- 342 UniProt Consortium. UniProt: the Universal Protein Knowledgebase in 2023. *Nucleic Acids Research*, 51(D1):
343 D483–D489, 2023. doi: 10.1093/nar/gkac1052.
- 344 Er-Jia Wang, Mary Barecki-Roach, and William W Johnson. Quantitative characterization of direct P-glycoprotein
345 inhibition by St John’s wort constituents hypericin and hyperforin. *Journal of Pharmacy and Pharmacology*, 56
346 (11):1451–1456, 2004. doi: 10.1211/0022357044736.
- 347 Reginald E Watkins, G Bruce Wisely, Linda B Moore, John L Collins, Millard H Lambert, Shawn P Williams,
348 Timothy M Willson, Steven A Kliewer, and Matthew R Redinbo. The human nuclear xenobiotic receptor PXR:
349 structural determinants of directed promiscuity. *Science*, 292(5525):2329–2333, 2001. doi: 10.1126/science.10
350 60762.

351 **Tables**

Table 1: **Network metrics reveal the instability of proximity Z-scores.** While Quercetin achieves more significant proximity Z-scores due to tighter null distributions, Hyperforin is physically closer (d_c) to DILI genes. Influence-based metrics resolve this confounding and stably prioritize Hyperforin. Network: STRING v12.0 LCC (confidence ≥ 900) filtered to liver-expressed genes.

Metric	Compound	Targets	Observed	Z	p	Efficiency
<i>Tier 1: Shortest-path proximity</i>						
	Hyperforin	10	$d_c = 1.30$	-3.86	< 0.001*	—
	Quercetin	62	$d_c = 1.68$	-5.44	< 0.001*	—
<i>Instability: Quercetin is physically more distant yet more "significant"</i>						
<i>Tier 2: Random walk influence (RWR)</i>						
	Hyperforin	10	0.1138	+10.12	< 0.001*	0.1138
	Quercetin	62	0.0322	+4.55	< 0.001	0.0322
<i>Resolution: Correctly prioritizes physical proximity and regulatory hub modulation</i>						
<i>Tier 3: Expression-weighted influence (EWI)</i>						
	Hyperforin	10	0.1330	+8.98	< 0.001*	0.1330
	Quercetin	62	0.0493	+5.79	< 0.001	0.0493

*At permutation floor (<1/1,000).

Efficiency = average influence per target; RWR = random walk with restart; EWI = expression-weighted influence; d_c = mean minimum shortest-path distance; DILI = drug-induced liver injury. All associations survived Benjamini–Hochberg FDR correction ($q < 0.05$).

Table 2: **Average influence efficiency.** Normalization to the total seeding mass quantifies the average influence per target. Hyperforin targets are 3.7-fold more efficient at perturbing the DILI module than Quercetin targets.

Analysis	Hyp. Eff.	Quer. Eff.	Eff. Ratio*	Rob. Ratio†
RWR (topology-only)	0.1138	0.0322	3.5×	3.7×
EWI (expression-weighted)	0.1330	0.0493	2.7×	2.8×

*Efficiency Ratio = Observed average influence ratio. †Robust Ratio = Observed influence / size-matched Bootstrap Mean (N=10). RWR = random walk with restart; EWI = expression-weighted influence.

Table 3: **Bootstrap sensitivity excludes target-count confounding.** Random 10-target subsets ($n = 100$) sampled without replacement from Quercetin’s 62-target pool. Hyperforin’s observed influence exceeds the entire bootstrap distribution.

Statistic	Value	Interpretation
Hyperforin observed	0.1138	Reference
Bootstrap mean	0.0308	Expected if targets equivalent
Bootstrap SD	0.0100	Sampling variability
Bootstrap 95% CI	[0.0160, 0.0542]	2.5th–97.5th percentile
Hyperforin / mean	3.7×	Effect size
Exceeds 95% CI?	Yes	Not attributable to sampling

Random seed: 42. Note: Bootstrap confirms robustness to target selection; it does not constitute independent inferential evidence.

Table 4: **Chemical similarity excludes structural confounding.** Neither compound resembles known hepatotoxins ($\text{Tanimoto} < 0.4$). Quercetin is more similar to DILI-positive drugs yet shows lower network influence.

Compound	Max Tanimoto (DILI+)	Max Tanimoto (DILI-)	Analog?*	Network rank
Hyperforin	0.154	0.202	No	1 (higher influence)
Quercetin	0.212	0.220	No	2 (lower influence)

*Analog threshold: $\text{Tanimoto} > 0.4$ (Maggiora et al., 2014). Morgan fingerprints (ECFP4, radius 2, 2048 bits). DILIrank: 542 DILI+, 365 DILI- drugs.

Table 5: **Hyperforin targets include regulatory hubs.** All 10 Hyperforin targets in the liver-expressed LCC, with liver expression (GTEx v8) and network degree. PXR (NR1I2) is the master regulator; CYP enzymes are downstream effectors.

Gene	Protein	TPM	Degree	Function	DILI link
NR1I2	PXR	43	28	Master regulator	Direct
CYP3A4	CYP3A4	335	89	Xenobiotic metabolism	Direct
CYP2C9	CYP2C9	434	76	Xenobiotic metabolism	Direct
CYP2B6	CYP2B6	125	42	Xenobiotic metabolism	Indirect
AKT1	PKB	33	312	Stress signaling	Indirect
ABCB1	P-gp	7	53	Drug efflux	Direct
ABCC2	MRP2	60	38	Drug efflux	Direct
ABCG2	BCRP	4	31	Drug efflux	Indirect
MMP2	MMP2	5	87	ECM remodeling	Indirect
MMP9	MMP9	1	94	ECM remodeling	Indirect

AKT1 is the highest-degree target (312 neighbors). Five of 10 targets (NR1I2, CYP3A4, CYP2C9, ABCB1, ABCC2) are directly connected to DILI genes. TPM = transcripts per million; DILI = drug-induced liver injury; LCC = largest connected component.

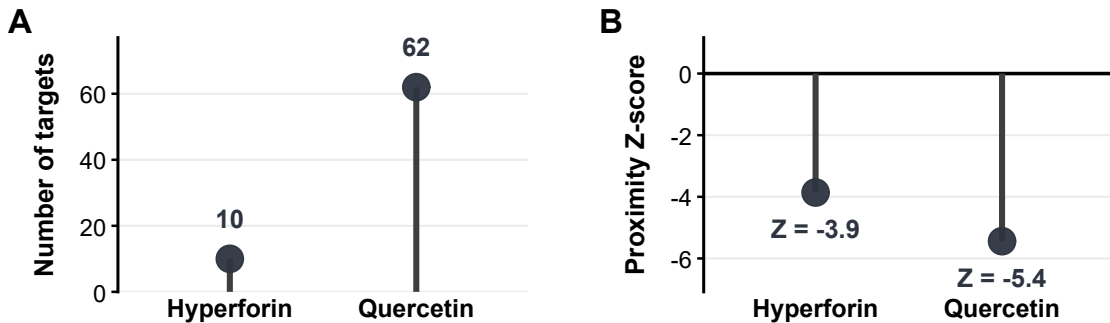
Table 6: **Influence ranking is robust to network construction parameters.** Hyperforin ranks first across all thresholds and influence metrics. Proximity Z-scores are unstable and reverse rankings between thresholds, failing to accurately reflect the physical distance advantage of Hyperforin.

Threshold	Compound	RWR Z	EWI Z	Proximity d_c	Proximity Z
≥ 700 (11,693 nodes)	Hyperforin	+12.08	+11.20	0.60	-6.04
	Quercetin	+5.53	+7.09	1.34	-5.46
≥ 900 (7,677 nodes)	Hyperforin	+10.12	+8.98	1.30	-3.86
	Quercetin	+4.55	+5.79	1.68	-5.44

Note: At ≥ 900 , Quercetin achieves a more "significant" proximity Z-score despite being physically more distant (1.68 vs 1.30) from DILI genes. RWR = random walk with restart; EWI = expression-weighted influence; d_c = mean minimum shortest-path distance; DILI = drug-induced liver injury.

352 **Figures**

Network context: target count and proximity to DILI genes

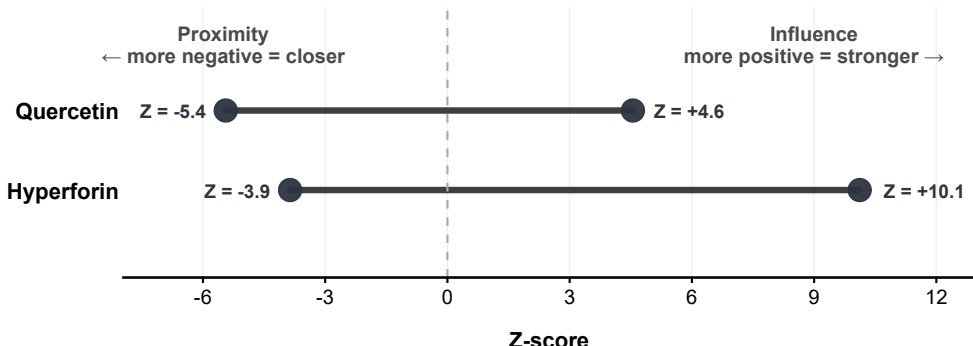


[DESCRIPTIVE CONTEXT] Target count and shortest-path proximity provide network context but are not used for causal inference. Proximity Z-scores represent deviation from degree-matched random expectation ($n = 1,000$ permutations). Negative values indicate closer-than-random proximity. Data: STRING v12.0 (≥ 900), human liver LCC.

Figure 1: Network context: target count and physical proximity to DILI genes. (A) Target count in the liver-expressed largest connected component. Quercetin: 62 targets; Hyperforin: 10 targets. (B) Shortest-path proximity (d_c) to 82 DILI-associated genes. Hyperforin is physically closer ($d_c = 1.30$) than Quercetin ($d_c = 1.68$). Z-scores represent deviation from degree-matched null expectation ($n = 1,000$ permutations). Quercetin: $Z = -5.44$ ($p < 0.001$); Hyperforin: $Z = -3.86$ ($p < 0.001$). Negative Z-scores indicate closer-than-random proximity. Network: STRING v12.0 (confidence ≥ 900), GTEx v8 (liver TPM ≥ 1).

Proximity does not predict influence

Proximity ranking is threshold-dependent; influence ranking is stable

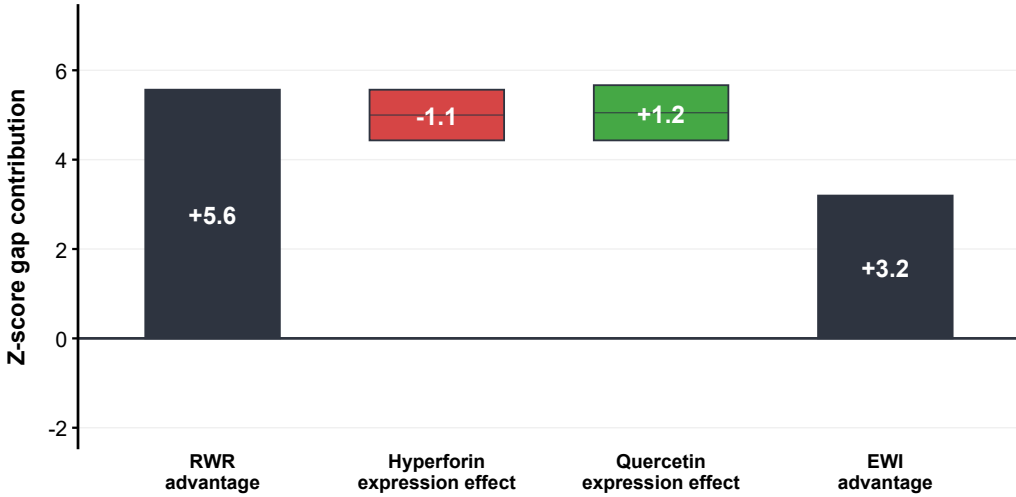


[CORE INFERENCE] The rank reversal demonstrates that shortest-path proximity does not predict functional influence. Lines connect each compound's proximity Z-score with its influence Z-score (random walk with restart, RWI). Both metrics derived from degree-matched permutation null models ($n = 1,000$). Data: STRING v12.0 (≥ 900).

Figure 2: **Instability of proximity Z-scores.** Dumbbell plot showing the dissociation between shortest-path proximity (left) and random walk influence (right) at STRING confidence ≥ 900 . At this threshold, Quercetin appears more "significant" in Z-score but is physically more distant (1.68 vs 1.30) from DILI genes. Hyperforin: proximity $Z = -3.86$, influence $Z = +10.12$ ($p < 0.001$). Quercetin: proximity $Z = -5.44$, influence $Z = +4.55$ ($p < 0.001$). Influence quantified by random walk with restart (RWR; $\alpha = 0.15$). $n = 1,000$ degree-matched permutations per compound.

Expression weighting attenuates but does not reverse the advantage

Gap: +5.6 (RWR) → +3.2 (EWI)

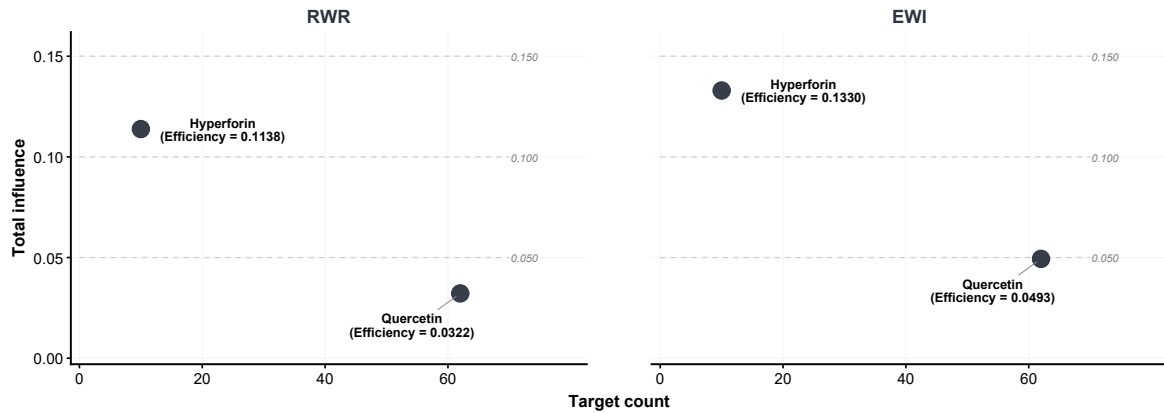


[CONSTRAINT ANALYSIS] The RWR advantage (+5.6) is partitioned under expression-weighted influence propagation:
 (1) Hyperforin's change under expression weighting (-1.1); (2) Quercetin's gain (+1.2, driven by CFB at 1115
 TPM). Residual advantage (+3.2) remains significant (both $p < 10^{-8}$). GTEx v8 liver expression (TPM ≥ 1). STRING
 v12.0 (≥ 900), $n = 1,000$ degree-matched permutations.

Figure 3: Expression weighting refines influence propagation. Waterfall decomposition of Z-score changes under expression-weighted influence (EWI). Initial Hyperforin advantage: $\Delta Z = +5.57$ (RWR). Hyperforin change: -1.14 (attenuation of signal through liver-active hubs). Quercetin change: $+1.24$ (gain from high-expression nodes like CFB). Residual Hyperforin advantage: $\Delta Z = +3.19$. Both compounds remain significant under EWI: Hyperforin $Z = +8.98$ ($p < 0.001$); Quercetin $Z = +5.79$ ($p < 0.001$). Expression weighting from GTEx v8 liver tissue.

Average network influence quantifies perturbation efficiency

Normalization reframes polypharmacology as efficiency, not coverage

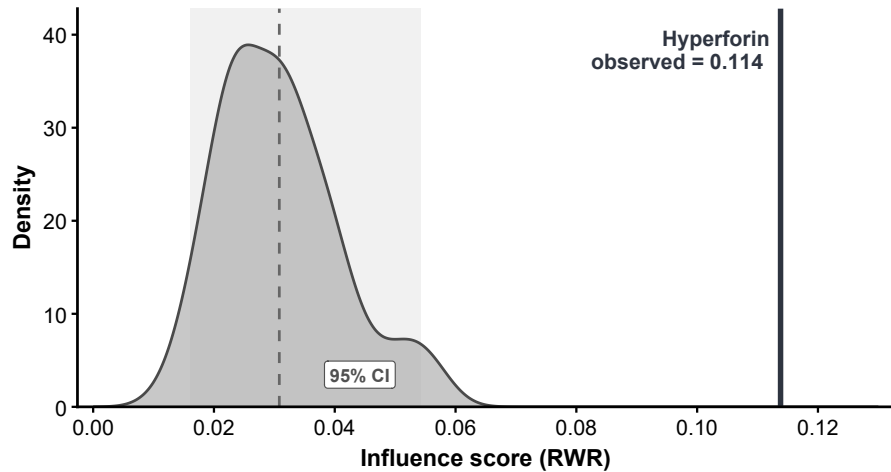


Average influence represents an effect-size normalization (total steady-state mass on DILI genes); no independent permutation test was performed. Horizontal lines represent efficiency tiers (Average Influence = constant). Hyperforin occupies a higher efficiency region despite fewer targets. Data: STRING v12.0 (≥ 900), $n = 1,000$ permutations.

Figure 4: Average network influence quantifies efficiency disparity. Phase plot of total influence versus target count. Horizontal lines represent efficiency tiers (Efficiency/average influence = constant). Hyperforin occupies a higher efficiency region despite fewer targets. Efficiency/average influence values: Hyperforin = 0.1138 (RWR), 0.1330 (EWI); Quercetin = 0.0322 (RWR), 0.0493 (EWI). Efficiency difference: **3.7 \times** (based on bootstrap mean comparison). The observed influence represents an effect-size normalization (total steady-state mass on DILI genes); no independent permutation test was performed.

Bootstrap sensitivity analysis excludes target-count confounding

Distribution of influence scores from random 10-target samples



[ROBUSTNESS CONTROL] Bootstrap sensitivity: 100 random 10-target samples from Quercetin's pool, scored by random walk with restart (RWI). Shaded = 95% CI. Hyperforin (solid line) exceeds entire distribution. Data: STRING v12.0 (≥ 900).

Figure 5: **Bootstrap sensitivity analysis excludes target-count confounding.** Density distribution of RWR influence scores from 100 random 10-target samples drawn from Quercetin's 62-target pool. Shaded region: 95% confidence interval (0.0160–0.0542). Vertical line: Hyperforin observed influence (0.1138). Hyperforin exceeds the entire bootstrap distribution (3.7× fold vs. mean). This confirms that Hyperforin's advantage is not attributable to favorable target count. Bootstrap is a robustness control; it does not provide independent statistical evidence.

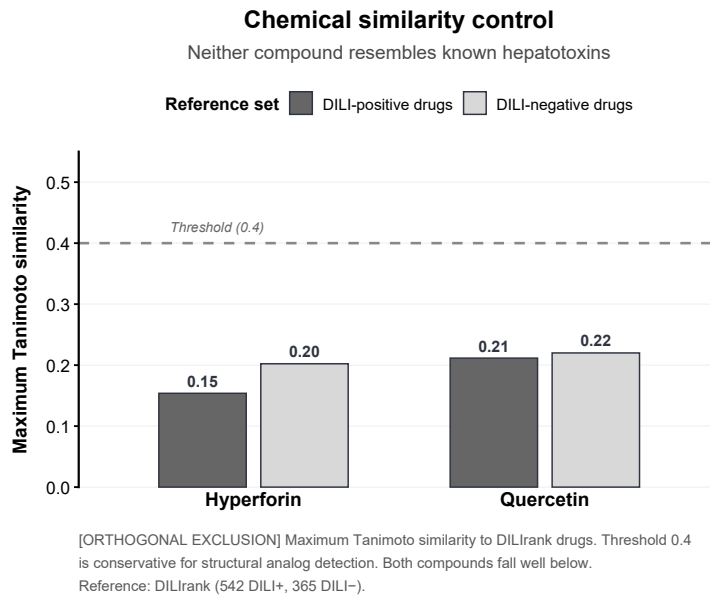


Figure 6: Chemical similarity control excludes structural confounding. Maximum Tanimoto similarity to DILIrack reference drugs. Reference set: 542 DILI-positive, 365 DILI-negative drugs. Hyperforin: max = 0.15 (DILI+), 0.20 (DILI-). Quercetin: max = 0.21 (DILI+), 0.22 (DILI-). Dashed line: 0.4 threshold for structural analog detection [Maggiora et al., 2014]. Neither compound is a structural analog of known hepatotoxins. This orthogonal analysis excludes chemical class as an explanation for the observed network signal. Fingerprints: Morgan (ECFP4), radius 2, 2048 bits.

353 **Declarations**

354 **Author Contributions (CRediT)**

355 **Antony Bevan:** Conceptualization, Methodology, Software, Validation, Formal analysis, Investigation, Data Cu-
356 ration, Writing - Original Draft, Writing - Review & Editing, Visualization.

357 **Use of AI Tools**

358 AI-assisted tools were used to assist with code development and statistical analysis. The author takes full respon-
359 sibility for all content.

360 **Competing Interests**

361 The author declares no competing interests.

362 **Data Availability**

363 All data and code supporting this study are publicly available at: <https://github.com/antonybevan/h-per>
364 foratum-network-tox

365 Source data for all figures and tables are provided in the Supplementary Information. Raw data were obtained
366 from the following public repositories:

- 367 • STRING v12.0: <https://string-db.org>
- 368 • GTEx v8: <https://gtexportal.org>
- 369 • ChEMBL v31: <https://www.ebi.ac.uk/chembl>
- 370 • DisGeNET: <https://www.disgenet.org>
- 371 • DILIrank 2.0: <https://www.fda.gov/science-research/ltrkb>

372 **Code Availability**

373 All analysis code is available at: <https://github.com/antonybevan/h-perforatum-network-tox>

374 The repository includes:

- 375 • Python scripts for network construction, RWR, permutation testing
- 376 • R scripts for visualization
- 377 • Complete pipeline documentation
- 378 • Fixed random seeds for full reproducibility

379 Software versions: Python 3.10, NetworkX 3.1, NumPy 1.26, Pandas 2.1, RDKit 2023.03, R 4.3, ggplot2 3.5.

³⁸⁰ **Funding**

³⁸¹ This research received no external funding.

³⁸² **Supplementary Tables**

Table 7: **Table S1. Hyperforin target genes and literature sources.** All 14 raw targets with UniProt IDs, gene symbols, and primary literature sources. Targets marked with * are present in the liver-expressed LCC (STRING ≥ 900 , GTEx TPM ≥ 1).

UniProt	Gene	In LCC	Source
O75469	NR1I2 (PXR)	Yes*	[Moore et al., 2000, Watkins et al., 2001]
P08684	CYP3A4	Yes*	[Moore et al., 2000]
P11712	CYP2C9	Yes*	[Obach, 2000]
P20813	CYP2B6	Yes*	[Komoroski et al., 2004]
P08183	ABCB1	Yes*	[Hennessy et al., 2002]
Q9UNQ0	ABCG2	Yes*	[Assefa and Butterweck, 2004]
O15440	ABCC2	Yes*	[Wang et al., 2004]
P31749	AKT1	Yes*	[Quiney et al., 2007]
P08253	MMP2	Yes*	[Quiney et al., 2007]
P14780	MMP9	Yes*	[Quiney et al., 2006]
Q9Y210	TRPC6	No	[Leuner et al., 2007]
P15692	VEGFA	No	[Quiney et al., 2006]
Q13794	PMAIP1	No	[Hostanska et al., 2003]
Q12879	GRIN1	No	[Kumar et al., 2006]

Table 8: **Table S2. Quercetin target curation summary.** Target counts at each processing stage.

Stage	Count
Raw targets (ChEMBL v31, CHEMBL159)	122
Excluded: non-human (mouse, rat, bacterial, viral)	10
Excluded: no UniProt mapping	25
Processed targets	87
Excluded: not liver-expressed (TPM < 1)	20
Excluded: not in STRING LCC	5
Final targets in LCC	62

Table 9: **Table S3. DILI gene set curation.** Genes associated with drug-induced liver injury from DisGeNET (UMLS C0860207).

Stage	Count
Raw DILI genes (DisGeNET)	127
In STRING ≥ 700 liver LCC	84
In STRING ≥ 900 liver LCC	82
Excluded: miRNAs (not in PPI network)	21
Excluded: cytokines (not in LCC)	12
Excluded: other	12

Table 10: **Table S4. Genes targeted by both compounds.** Five genes present in both Hyperforin and Quercetin target sets.

Gene	Protein	Function
ABCG2	BCRP	Efflux transporter
AKT1	Protein kinase B	Cell survival signaling
CYP3A4	Cytochrome P450 3A4	Drug metabolism
MMP2	Matrix metalloproteinase-2	Extracellular matrix remodeling
MMP9	Matrix metalloproteinase-9	Extracellular matrix remodeling

Table 11: **Table S5. Direct DILI gene connectivity.** Hyperforin targets with first-order (distance = 1) connections to DILI genes in the STRING network (≥ 900). DILI neighbors are genes present in the 82-gene DILI set.

Target	DILI Neighbors	N	Function
CYP3A4	NR1I2, CYP2E1, UGT1A9, GSTM1, GSTP1	5	Xenobiotic metabolism
AKT1	MAP3K5, NFE2L2, CTNNB1, IGF1	4	Stress response
MMP9	LCN2, SPP1, MMP2	3	Inflammation/ECM
ABCB1	ABCC2, NR1I2	2	Drug transport
CYP2C9	CYP2E1, NR1I2	2	Xenobiotic metabolism
CYP2B6	NR1I2	1	Xenobiotic metabolism
NR1I2	CYP2E1, ABCC2	2	Master regulator
ABCG2	ABCC2	1	Drug transport
ABCC2	NR1I2, ABCB1	2	Drug transport
MMP2	MMP9, SPP1	2	ECM remodeling
Total unique		12	

Table 12: **Table S6. Quercetin direct DILI gene connectivity summary.** Summary statistics for first-order DILI connections across Quercetin's 62 targets.

Metric	Value
Total targets in LCC	62
Targets with ≥ 1 direct DILI neighbor	18
Total direct DILI connections	31
Mean DILI neighbors per target	0.50
<i>Hyperforin comparison:</i>	
Hyperforin targets with ≥ 1 DILI neighbor	10/10 (100%)
Mean DILI neighbors per Hyperforin target	2.4

Table 13: **Table S7. Quercetin target genes in the liver-expressed network.** All 62 Quercetin targets in STRING v12.0 LCC (confidence ≥ 900) with liver TPM ≥ 1 (GTEX v8). Sorted by descending liver expression.

Gene	TPM	Gene	TPM	Gene	TPM	Gene	TPM
CFB	1115	CYP3A4	335	FN1	229	ALDH2	183
ANPEP	160	PPIA	112	SERPINA5	104	CYP1A2	72
CA2	64	APP	63	PYGL	55	HDAC6	45
ESRRRA	42	MAOA	35	AKR1C2	33	AKT1	33
CTSH	28	XDH	26	CHRNA4	25	PIK3R1	24
PIM1	24	LDLR	23	EGFR	17	ELOVL1	18
PKN1	16	GSK3A	13	YES1	13	MET	12
DAPK1	12	BACE1	11	CSNK2A1	10	FSTL1	9
SIRT6	8	GSK3B	7	CDK7	7	CAV2	7
PTPN2	6	CYP1A1	5	PRMT7	5	MMP2	5
AKR1B1	5	PDE6D	5	PTK2	4	ABCG2	4
IQGAP1	4	ADRB2	3	BRAF	4	KDR	3
SRC	3	ALOX5	3	CYP1B1	3	TLR4	3
NUAK1	3	AXL	2	ADA	2	LCK	2
ABCC1	2	PLK1	1	ACHE	1	MMP9	1
SYK	1	PDZK1IP1	1				

Table 14: **Table S8. DILI gene set (82 genes).** Genes in STRING v12.0 LCC (confidence ≥ 900) with liver TPM ≥ 1 (GTEX v8). Source: DisGeNET (UMLS C0860207). Sorted alphabetically.

82 DILI-Associated Genes							
ABCB1	AHR	ALB	ALDOB	AMBP	APOA1	APOE	APOH
ARG1	ARNT	ATG5	BAX	BTD	C3	CAT	CCL2
CLU	COL3A1	CTNNB1	CXCL1	CXCL10	CYP2A6	CYP2C19	CYP2C9
CYP2E1	DGAT2	ENO1	FGA	FLT1	FMO3	GADD45A	GC
GCLC	GPT	GSN	GSTM1	GSTM2	GSTP1	HLA-A	HLA-B
HLA-DQB1	HLA-DRB1	HMGB1	HMOX1	HPD	HPX	IGF1	IL18
IL1R2	KRT18	LCN2	LGALS3	MAP3K5	MED1	MMP2	MTHFR
NAT2	NFE2L2	NR1H3	NR1H4	NR1I2	NR1I3	PLAT	PLG
PNP	POLG	PON1	PPARA	PRKDC	PTGS2	RBP1	SLPI
SNX18	SOD1	SOD3	SPP1	TALDO1	TBXA2R	TCTN1	TF
TTR	UGT1A9						

Table 15: **Table S9. Null distribution parameters from permutation testing.** Null distribution parameters (mean and standard deviation) from $n = 1,000$ degree-matched permutations. Note the tightening of the Quercetin null distribution as the number of targets increases, which drives the inflation of proximity Z-scores.

Metric	Compound	μ_{null}	σ_{null}	x_{obs}	Z-score
<i>Shortest-path proximity (at ≥ 900)</i>					
	Hyperforin (10)	2.21	0.235	1.30	-3.86
	Quercetin (62)	2.17	0.091	1.68	-5.44
<i>Random walk influence (at ≥ 900)</i>					
	Hyperforin (10)	0.0147	0.0098	0.1138	+10.12
	Quercetin (62)	0.0148	0.0038	0.0322	+4.55
<i>Expression-weighted influence (at ≥ 900)</i>					
	Hyperforin (10)	0.0205	0.0125	0.1330	+8.98*
	Quercetin (62)	0.0209	0.0049	0.0493	+5.79*

*Significance remains high despite tissue-specific attenuation. μ_{null} = null distribution mean; σ_{null} = null distribution standard deviation; x_{obs} = observed metric value.